Contribution from the Department of Chemistry, The University of Iowa, Iowa City, Iowa 52242, and Nuclear Research Center, "Demokritos", Aghia Paraskevi, Attiki, Greece

Trinuclear Fe–M–S Complexes Containing a Linear Fe–M–Fe Array and a Bridging S_2MS_2 Unit. Electronic Structures and Crystal and Molecular Structures of the $[(C_6H_5)_4P]_2[Cl_2FeS_2MS_2FeCl_2]$ (M = Mo, W) Complexes

D. COUCOUVANIS,*[1] E. D. SIMHON, P. STREMPLE, M. RYAN, D. SWENSON, N. C. BAENZIGER, A. SIMOPOULOS, V. PAPAEFTHYMIOU, A. KOSTIKAS, and V. PETROULEAS

Received August 26, 1983

The title complexes $[Cl_2FeS_2MS_2FeCl_2]^{2-}$ (M = Mo (I), W (II)) are obtained either by oxidation of the $[(PhS)_2FeS_2MS_2]^{2-}$ complexes with $FeCl_3 \cdot 6H_2O$ or by direct syntheses from $FeCl_2$ and the MS_4^{2-} anions in acetonitrile solution. Complexes I and II undergo dissociation in donor solvents with loss of $FeCl_2$ and formation of the dinuclear $[Cl_2FeS_2MoS_2]^{2-}$ complexes. The $(C_6H_5)_4P^+$ salt of the $[Cl_2FeS_2MoS_2FeCl_2]^{2-}$ anion (I) crystallizes in the triclinic space group $P\bar{1}$ with two molecules per unit cell. The cell dimensions for I are a = 10.197 (2) Å, b = 13.054 (2) Å, c = 20.164 (3) Å, α = 100.46 (2)°, β = 100.61 (1)°, and γ = 100.92 (1)°. The tungsten complex $[(C_6H_5)_4P]_2[Cl_2FeS_2WS_2FeCl_2]$ (II) is X-ray isomorphous and isostructural. The cell dimensions for II are a = 10.215 (6) Å, b = 13.071 (5) Å, c = 20.187 (7) Å, α = 100.54 (3)°, β = 100.58 (2)°, and γ = 100.97 (2)°. Intensity data for I and II were collected with a four-circle computer-controlled diffractometer with use of the θ–2θ scan technique. In all structures, all non-hydrogen atoms were refined with anisotropic temperature factors and the hydrogen atoms were included in the structure factor calculations but not refined. Refinement by full-matrix least squares of 550 parameters on 5125 data for I and 550 parameters on 9711 data for II gave final R values of 0.058 and 0.050, respectively. The structures of these trinuclear complexes consist of a tetrahedral MS_4^{2-} unit bridging two $FeCl_2$ groups. The Fe–Mo distances in I at 2.771 (2) and 2.781 (2) Å and the Fe–Fe distance at 5.552 (2) Å are all shorter than the corresponding distances in II, which are 2.795 (1), 2.808 (1), and 5.603 (1) Å, respectively. The Fe–M–Fe angles in I and II are 179.37 (6) and 179.25 (4)°, respectively. Average values of other structural parameters are as follows: for I, Fe–S = 2.296 (4) Å, Fe–Cl = 2.234 (1) Å, Mo–S = 2.206 (2) Å, Fe–S_b–Mo = 76.1 (1)°; for II, Fe–S = 2.320 (6) Å, Fe–Cl = 2.233 (10) Å, W–S = 2.209 (5) Å, Fe–S_b–W = 76.4 (2)°. The structural as well as Mössbauer and magnetic properties of I and II indicate that the WS_4^{2-} unit is a weaker bridging ligand than MoS_4^{2-}. Chemical and electrochemical studies show that I and II undergo a one-electron reduction followed by loss of Cl^- and formation of the $([Fe_2Cl_3S_2MS_2]^{2-})_x$ anions.

Introduction

Direct structural information and spectroscopic data available for the Fe–Mo site in the nitrogenase enzymes[2] have stimulated considerably activity in the synthesis of Fe–Mo–S clusters. The structural information for nitrogenase has been obtained from X-ray absorption spectroscopy and in particular from the analysis of Mo EXAFS (extended X-ray absorption fine structure). In the Fe–Mo protein of nitrogenase, the Mo EXAFS data[3] are consistent with the presence of Mo in (a) a high-sulfur, non-oxo environment (~4–5 S atoms at ~2.36 Å from the Mo atom) and (b) close proximity to two or three Fe atoms at distances (~2.72 Å) compatible with Fe–S–Mo bridging units. Either of the two proposed[3] models, for the nitrogenase Mo site (Figure 1), could be a structural feature of the active site.

The nature of the active site is defined further by recent results of Mössbauer and EPR spectroscopic studies[4] on the Fe–Mo protein and the Fe–Mo cofactor from *A. vinelandii*. Analyses of these results suggest the presence of Fe–Mo, $S = {}^3/_2$ centers (M centers) that contain one Mo and five to seven Fe atoms in a spin-coupled structure. The use of pulsed EPR spectroscopy on ^{95}Mo- ($I = {}^5/_2$) and ^{96}Mo- ($I = 0$) enriched Fe–Mo protein and spin-echo amplitude measurements[5] reaffirm that the Mo is a component of the $S = {}^3/_2$ system.

The basic approaches that have been followed in the synthesis of heterometallic Fe–Mo–S complexes as active-site analogues can be classified into two general categories: the spontaneous self-assembly reactions[6] and the MS_4^{2-}–$Fe(L)_n$ ligand-exchange reactions (M = Mo, W). The former is based on the hypothesis that metalloprotein active-site analogues may be thermodynamically favored reaction products in mixtures of appropriate reactants, while the latter is based on the demonstrated ability of the MS_4^{2-} anions to serve as ligands for transition-metal ions.[7]

Various Fe–Mo–S clusters form spontaneously and can be isolated from mixtures of MoS_4^{2-}, $FeCl_3$, and NaSR. The first examples of these clusters, which contained the $Mo_2Fe_6S_{11}$ framework, were isolated and characterized independently by two groups who communicated their results at approximately the same time for $[M_2Fe_6S_9(SR)_8]^{3-}$ (M = Mo, W; R = Et[8])

(1) Present permanent address: Department of Chemistry, University of Michigan, Ann Arbor, MI 48109.

(2) (a) Eady, R. R.; Smith, B. E. In "A Treatise on Dinitrogen Fixation"; Hardy, R. W. F., Bottomley, F., Burns, R. C., Eds.; Wiley-Interscience: New York, 1979; Chapter 2 (Section II). (b) Orme-Johnson, W. H.; Davis, L. C. In "Iron-Sulfur Proteins"; Lovenberg, W., Ed.; Academic Press: New York, 1977; Vol. 3, Chapter 2.

(3) (a) Cramer, S. P.; Hodgson, K. O.; Gillum, W. O.; Mortenson, L. E. *J. Am. Chem. Soc.* **1978**, *100*, 3398. (b) Cramer, S. P.; Gillum, W. O.; Hodgson, K. O.; Mortenson, L. E.; Stiefel, E. I.; Chisnel, J. R.; Brill, W. J.; Shah, V. K. *Ibid.* **1978**, *100*, 3814. (c) Burgess, B. K.; Yang, S. S.; You, C. B.; Li, J. G.; Friesen, G. D.; Pan, W. H.; Stiefel, E. I.; Newton, W. E.; Conradson, S. D.; Hodgson, K. O. "Current Perspectives in Nitrogen Fixation"; Gibson, A. H., Newton, W. E., Eds.; Elsevier/North-Holland Press: New York, 1981; p 71. The most recent Mo EXAFS analysis of FeMoCo shows, in addition to the Fe and S near neighbors, two of three oxygen (or nitrogen) ligands at 2.10 Å from the molybdenum. This feature, which is not present in the Mo EXAFS of the Fe–Mo protein of nitrogenase, very likely arises as a result of the FeMoCo isolation procedure and suggests NMF coordination to the Mo atom.

(4) (a) Rawlings, J.; Shah, V. K.; Chisnell, J. R.; Brill, W. J.; Zimmermann, R.; Münck, E.; Orme-Johnson, W. H. *J. Biol. Chem.* **1978**, *253*, 1001. (b) Orme-Johnson, W. H.; Orme-Johnson, N. R.; Touton, L.; Emptage, M.; Henzl, M.; Rawlings, J.; Jakobson, K.; Smith, J. P.; Mims, W. B.; Huynh, B. H.; Münck, E.; Jacob, G. S. In "Molybdenum Chemistry of Biological Significance"; Newton, W. E., Otsuka, S., Eds.; Plenum Press: New York, 1979; p 85 and references therein.

(5) (a) Hoffman, B. M.; Roberts, J. E.; Orme-Johnson, W. H. *J. Am. Chem. Soc.* **1982**, *104*, 860–862. (b) Hoffman, B. M.; Venters, R. A.; Roberts, J. E.; Nelson, M.; Orme-Johnson, W. H. *Ibid.* **1982**, *104*, 4711–4712.

(6) Holm, R. H. *Chem. Soc. Rev.* **1982**, *11*, 455–490.

(7) Diemann, E.; Muller, A. *Coord. Chem. Rev.* **1973**, *10*, 79.

0020-1669/84/1323-0741$01.50/0

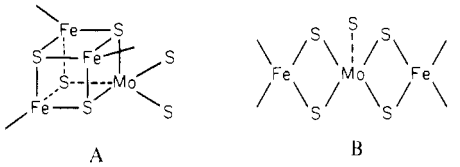

Figure 1. Proposed models for the Mo coordination environment in nitrogenase.[3a]

and for $[M_2Fe_6S_8(SR)_9]^{3-}$ (M = Mo, W, R = Et;[8] M = Mo, R = Ph[9,10]). Subsequent to these reports variants and derivatives of these molecules have been reported that contain as a common feature the Fe_3MoS_4 unit (Figure 1A). Among these are included $[Mo_2Fe_6S_8(SPh)_9]^{5-}$,[11a] $[Mo_2Fe_6S_8(\mu\text{-}OMe)_3(SPh)_6]^{3-}$,[10a] $[Mo_2Fe_7S_8(SR)_{12}]^{3-}$,[11b] $[Mo_2Fe_7S_8(SR)_{12}]^{4-}$,[11b] $[MoFe_4S_4(SC_2H_5)_3(C_6H_4O_2)_3]^{3-}$,[11d] and $[MoFe_3S_4(S\text{-}p\text{-}C_6H_4Cl)_4((C_3H_5)_2cat)]^{3-}$.[11e]

The MS_4^{2-}–$Fe(L)_n$ (M = Mo, W) ligand-exchange reactions have led to the synthesis of numerous oligonuclear Fe–Mo–S complexes of the general type $[(MS_4)Fe(L)_n]^{n-}$ (M = Mo, W, L = PhS^-, n = 2;[12a,13] M = Mo, W, $(L)_n$ = S_5^{2-}, n = 2;[12b] M = Mo, W, L = Cl, n = 2;[14,15] M = Mo, W, L = NO, N = 2;[16] M = Mo, W, $(L)_n$ = MS_4^{2-}, n = 3).[17,18] Of these dinuclear anions, which can only be considered as elementary units for the eventual synthesis of larger Fe–Mo–S aggregates, the $[(RS)_2FeMS_4]^{2-}$ and $[Cl_2FeS_2MS_2]^{2-}$ complexes have been used in the synthesis of the trinuclear $[Cl_2FeS_2MS_2FeCl_2]^{2-}$ anions, which contain the linear FeS_2MoS_2Fe center (Figure 1B).

Thus far, the stoichiometric requirements (Fe:Mo:S ratio of (6 ± 1):1:4) dictated by the available data for the Fe–Mo–S core in either nitrogenase or the Fe–Mo cofactor[19] are not met in any of the available Fe–Mo–S "analogue" complexes. However, in the structures of the double cubanes and of the $[Cl_2FeS_2MoS_2FeCl_2]^{2-}$ complex,[14] the $MoFe_3S_4$ and FeS_2MoS_2Fe cores represent the first structural models for the immediate Mo coordination environments suggested by and compatible with the EXAFS analyses (Figure 1).

In this paper we report in detail on the synthesis, structural characterization, and electronic properties of the $[Cl_2FeS_2MS_2FeCl_2]^{2-}$ anions.

Experimental Section

Methods and Materials. The syntheses of all complexes were performed under a pure dinitrogen atmosphere in a Vacuum Atmospheres Dri-Lab glovebox. Chemicals generally were used as purchased. Commercial grade dichloromethane (CH_2Cl_2) and acetonitrile (CH_3CN) were distilled from calcium hydride. Dimethylformamide (DMF) was dried over Linde 4A molecular sieves for 24 h and then distilled under reduced pressure at 30 °C. Absolute ethanol and diethyl ether were used without any further purification. The "inert"-atmosphere gases (Ar, N_2) were purified by passing them through a H_2-reduced CuX ("De-ox") deoxygenation catalyst tower and, immediately after, through a sodium hydroxide pellet tower.

Physical Measurements. Mössbauer spectra were measured from 1.1 K to room temperature with a constant-acceleration spectrometer. The source was 100 mCi of ^{57}Co in a Rh matrix and was held at room temperature. Measurements also were made with the absorber in external magnetic fields up to 65 kOe with a superconducting magnet operating in a transverse configuration. Magnetic susceptibility measurements were carried out with a vibrating sample magnetometer from 4.2 K to room temperature. Visible and ultraviolet spectra were obtained on Cary Model 118 and 219 spectrophotometers. Solution near-infrared spectra were obtained on a Beckman DK-2 spectrophotometer.

Electrochemical measurements were performed with a PAR Model 173 potentiostat/galvanostat and a PAR Model 175 universal programmer. The electrochemical cells used had either platinum or hanging-mercury-drop working electrodes and platinum auxiliary electrodes. As reference electrode a saturated calomel electrode was used. All solvents used in the electrochemical measurements were properly dried and distilled, and tetra-*n*-butylammonium perchlorate (Bu_4NClO_4) was used as the supporting electrolyte. Purified dinitrogen or argon was used to purge the solutions prior to the electrochemical measurements. Powder diffraction diagrams were obtained by using a 114-mm diameter Debye–Scherrer type camera with Ni-filtered Cu Kα radiation (λ = 1.5418 Å).

Synthesis. Bis(tetraphenylphosphonium) Tetrakis(μ-thio)[bis(dichloroferrate(II))molybdate(VI)], $(Ph_4P)_2(Cl_2FeS_2MoS_2FeCl_2)$. Method A. An amount of $(Ph_4P)_2[(PhS)_2FeS_2MoS_2]$ (1.79 g, 1.5 mmol) is dissolved in a minimum volume of DMF. To this solution is added a DMF solution containing 0.83 g of $FeCl_3{\cdot}6H_2O$ (3 mmol) with constant stirring. After ca. 10 min the orange solution is filtered and the filtrate flooded with diethyl ether. The dark red oil that separates out is kept and the supernatant solution discarded. The oil solidifies upon repeated washings and scratchings. The solid is dried and redissolved in a minimum amount of DMF.

A few drops of absolute ethanol and diethyl ether are added until a flocculent precipitate appears. At this stage the solution is filtered, and to the filtrate is added diethyl ether to incipient crystallization. After 1 h, 1.18 g of crystalline product is isolated; yield 57%. Anal. Calcd for $Fe_2MoCl_4S_4P_2C_{48}H_{40}$ (mol wt 1156.5): C, 49.85; H, 3.49; P, 5.36; S, 11.09; Cl, 12.26; Fe, 9.66; Mo, 8.30. Found: C, 49.69; H, 3.42; P, 5.36; S, 10.94; Cl, 11.60; Fe, 9.30.

Method B. An amount of $FeCl_2{\cdot}4H_2O$ (1.98 g, 10 mmol) is dissolved in a minimum amount of DMF. To this solution is added a solution of 3.76 g (10 mmol) of Ph_4PCl in 10 mL of DMF with stirring and, shortly thereafter, a solution of 1.3 g of $(NH_4)_2MoS_4$ (5 mmol) in 5 mL of DMF. After it was stirred for ca. 5 min, the orange solution is filtered and to the filtrate are added a few drops of absolute ethanol. Diethyl ether is added to incipient crystallization, and the contents are allowed stand for 0.5 h. The crystalline material is isolated, washed with diethyl ether, and dried in vacuo. The properties of the product are identical with those of the product obtained by method A.

Bis(tetraphenylphosphonium) Bis(μ-thio)[dichloroferrate(II)dithiomolybdate(VI)], $(Ph_4P)_2(Cl_2FeS_2MoS_2)$. An amount of $(Ph_4P)_2[Cl_2FeS_2MoS_2FeCl_2]$ (1.76 g, 1.5 mmol) is dissolved in a minimum volume of DMF (~10 mL), and to the resulting orange solution is added a solution of 1.35 g of $(Ph_4P)_2MoS_4$ (1.5 mmol) in

(8) (a) Wolff, T. E.; Power, P. P.; Frankel, R. B.; Holm, R. H. *J. Am. Chem. Soc.* **1980**, *102*, 4694–4703. (b) Wolff, T. E.; Berg, J. M.; Hodgson, K. O.; Frankel, R. B.; Holm, R. H. *Ibid.* **1979**, *101*, 4140–4150.
(9) (a) Christou, G.; Garner, C. D.; Mabbs, F. E. *Inorg. Chim. Acta* **1978**, *28*, L189. (b) Christou, G.; Garner, C. D.; Mabbs, F. E.; King, T. J. *J. Chem. Soc., Chem. Commun.* **1984**, 740. (c) Christou, G.; Garner, C. D.; Miller, R. M.; Johnson, C. E.; Rush, J. D. *J. Chem. Soc., Dalton Trans.* **1980**, 2363–2368.
(10) Christou, G.; Garner, C. D. *J. Chem. Soc., Dalton Trans.* **1980**, 2354–2362.
(11) (a) Christou, G.; Mascharak, P. M.; Armstrong, W. H.; Papaefthymiou, A. C.; Frankel, R. B.; Holm, R. H. *J. Am. Chem. Soc.* **1982**, *104*, 2820–2831. (b) Nolff, T. E.; Berg, J. M.; Power, P. P.; Hodgson, K. O.; Holm, R. H. *Inorg. Chem.* **1980**, *19*, 430–437. (c) Armstrong, W. H.; Mascharak, P. K.; Holm, R. H. *J. Am. Chem. Soc.* **1982**, 4373–4383. (d) Wolff, T. E.; Berg, J. M.; Holm, R. H. *Inorg. Chem.* **1981**, *20*, 174. (e) Mascharak, P. K.; Armstrong, W. H.; Mizobe, Y.; Holm, R. H. *J. Am. Chem. Soc.* **1983**, *105*, 475.
(12) (a) Coucouvanis, D.; Simhon, E. D.; Swenson, D.; Baenziger, N. C. *J. Chem. Soc., Chem. Commun.* **1979**, 361. Coucouvanis, D.; Stremple, P.; Simhon, E. D.; Swenson, D.; Baenziger, N. C.; Draganjac, M.; Chan, L. T.; Simopoulos, A.; Papaefthymiou, V.; Kostikas, A.; Petrouleas, V. *Inorg. Chem.* **1983**, *22*, 293–308. (b) Coucouvanis, D.; Baenziger, N. C.; Simhon, E. D.; Stremple, P.; Swenson, D.; Kostikas, A.; Simpoulos, A.; Petrouleas, V.; Papaefthymiou, V. *J. Am. Chem. Soc.* **1980**, *102*, 1730.
(13) Tieckelmann, R. H.; Silvis, H. C.; Kent, T. A.; Huynk, B. H.; Waszcak, J. V.; Teo, B.-K.; Averill, B. A. *J. Am. Chem. Soc.* **1980**, *102*, 5550.
(14) Coucouvanis, D.; Baenziger, N. D.; Simhon, E. D.; Stremple, P.; Swenson, D.; Simopoulos, A.; Kostikas, A.; Petrouleas, V.; Papaefthymiou, V. *J. Am. Chem. Soc.* **1980**, *102*, 1732.
(15) Müller, A.; Tölle, H.-G.; Bögge, H. *Z. Anorg. Allg. Chem.* **1980**, *115*, 471.
(16) Coucouvanis, D.; Simhon, E. D.; Stremple, P.; Baenziger, N. C. *Inorg. Chim. Acta* **1981**, *53*, L135–137.
(17) Coucouvanis, D.; Simhon, E. E.; Baenziger, N. C. *J. Am. Chem. Soc.* **1980**, *102*, 6644.
(18) McDonald, J. W.; Friesen, G. D.; Newton, W. E. *Inorg. Chim. Acta* **1980**, *46*, L79.
(19) (a) Shah, V. K.; Brill, W. J. *Proc. Natl. Acad. Sci. U.S.A.* **1977**, *74*, 3249. Smith, B. E. In "Molybdenum Chemistry of Biological Significance"; Newton, W. E., Otsuka, S., Eds.; Plenum Press: New York, 1980; p 179.

10 mL of DMF with stirring. Following filtration, diethyl ether is added to the solution, and the crystalline red product precipitates out. Recrystallization of the crude product from a DMF–ether mixture affords analytically pure material; yield 75%. Anal. Calcd for $FeMoCl_2S_4P_2C_{48}H_{40}$ (mol wt 1029.7): C, 55.98; H, 3.89; P, 6.02; S, 12.45; Cl, 6.88; Fe, 5.43; Mo, 9.32. Found: C, 55.76; H, 4.04; Fe, 5.43; Mo, 9.32.

Bis(tetraphenylphosphonium) Tetrakis(μ-thio)[bis(dichloroferrate(II))tungstate(VI)], $(Ph_4P)_2(Cl_2FeS_2WS_2FeCl_2)$. Method A. An amount of $(Ph_4P)_2[(PhS)_2FeS_2WS_2]$ (1 g, 0.79 mmol) is dissolved in 45 mL of CH_3CN. To the red solution is added a solution of 0.42 g (1.6 mmol) of $FeCl_3·6H_2O$ in 10 mL of CH_3CN. The solution is stirred for ca. 10 min during which time the color changes to dark olive green and eventually to deep golden yellow. The solution is filtered, and 5 mL of absolute ethanol is added, followed by the slow addition of diethyl ether until the total solution volume is 300 mL. When it is allowed to stand, the product crystallizes as golden yellow microcrystals. The crystals are isolated by filtration, washed with two 15-mL portions of diethyl ether, and dried in vacuo; yield 0.83 g (0.67 mmol, 84%). Anal. Calcd for $Fe_2WCl_4S_4P_2C_{48}H_{40}$: C, 46.34; H, 3.24; S, 10.30; W, 14.77; Cl, 11.39. Found: C, 46.23; H, 3.32; S, 10.35; W, 14.45; Cl, 11.57.

Method B. An amount of $(Ph_4P)_2Cl_2FeS_2WS_2$ (1 g, 0.89 mmol) and $FeCl_2$ (0.11 g, 0.89 mmol) is added to 30 mL of CH_3CN, and the mixture is allowed to stir for 30 min. Following filtration, 5 mL of absolute ethanol is added to the solution. Diethyl ether is slowly added to precipitate the product as golden yellow microcrystals. The crystals are washed with two 10-mL portions of diethyl ether and dried in vacuo; yield 1.05 g (0.84 mmol, 94%). The properties of this material are identical with those of the product obtained by method A.

Bis(tetraphenylphosphonium) Bis(μ-thio)[dichloroferrate(II)dithiotungstate(VI)], $(Ph_4P)_2(Cl_2FeS_2WS_2)$. Method A. To 25 mL of DMF is added 1 g of $(NH_4)_2WS_4$ (2.87 mmol), 0.36 g of $FeCl_2$ (2.87 mmol), and 2.14 g of Ph_4PCl (5.74 mmol). The solution is stirred for 15 min during which time the color changes from yellow to red. A light white solid (NH_4Cl) is isolated by filtration, and to the filtrate is added 5 mL of absolute ethanol. Slow addition of diethyl ether causes the product to precipitate as red-orange microcrystals. Following filtration, the crystals are washed with two 15-mL portions of diethyl ether and dried in vacuo; yield 3.09 g (2.76 mmol, 96%). The product can be recrystallized from DMF–ether mixtures. Anal. Calcd for $FeWCl_2S_4P_2C_{48}H_{40}$ (mol wt 1117.26): C, 51.55; H, 3.60; S, 11.47; Cl, 6.34; Fe, 4.99; W, 16.45. Found: C, 51.45; H, 3.71; S, 11.31; Cl, 6.51; Fe, 4.80; W, 16.48.

Method B. To 20 mL of dry CH_3CN are added 0.85 g of $(Ph_4P)_2Cl_2FeS_2WS_2FeCl_2$ (0.68 mmol) and 0.67 g of $(Ph_4P)_2WS_4$ (0.68 mmol). The mixture is stirred for 10 min and then filtered. Upon addition of ether to the filtrate to incipient crystallization and standing, orange crystals form. The crystals are collected by filtration, washed with two 10-mL portions of diethyl ether, and dried in vacuo; yield 1.45 g (95%).

Bis(tetraethylammonium) Tetrakis(μ-thio)[bis(dichloroferrate(II))molybdate(VI)], $(Et_4N)_2(Cl_2FeS_2MoS_2FeCl_2)$. An amount of $(Et_4N)_2MoS_4$ (1.0 g, 2.1 mmol) is dissolved in 35 mL of CH_3CN. To the intensely red solution is added 0.525 g (4.2 mmol) of anhydrous $FeCl_2$. The solution is stirred for 2 h and filtered. Diethyl ether is added to the filtrate, and $(Et_4N)_2(Cl_2FeS_2MoS_2FeCl_2)$ is obtained as yellow-brown crystals. The physical properties of this material (IR and electronic spectra) are as expected; yield 1.27 g (1.72 mmol, 84%). Anal. Calcd: C, 26.04; H, 5.46; N, 3.82. Found: C, 25.90; H, 5.65; N, 4.12. The corresponding tungsten complex can be obtained in a similar manner using $(Et_4N)_2WS_4$.

$((Et_4N)_2MoS_4Fe_2Cl_3)_x$. An amount of $(Et_4N)_2(Cl_2FeS_2MoS_2FeCl_2)$ (0.400 g, 0.54 mmol) is dissolved in 50 mL of CH_3CN. The solution is filtered, and 0.085 g (0.59 mmol) of solid $(Et_4N)BH_4$ is added slowly with stirring. The purple microcrystalline product precipitates out over a 2-h period and is isolated by filtration. It can be washed with CH_2Cl_2 and dried in vacuo. The yield is essentially quantitative. The product can be recrystallized from a DMF–ether mixture and is isolated as a DMF solvate. Anal. Calcd for $Fe_2MoCl_3S_4N_2C_{16}H_{40}$: C, 28.43; H, 5.89; N, 4.74; Cl, 14.42; S, 17.33; Fe, 15.12; Mo, 12.94. Found: C, 28.30; H, 5.98; N, 4.75; Cl, 13.47; S, 17.96; Fe, 13.92; Mo, 12.81.

$((Et_4N)_2WS_4Fe_2Cl_3)_x$. An amount of $(Et_4N)_2(Cl_2FeS_2WS_2FeCl_2)$ (0.400 g, 0.48 mmol) is dissolved in 100 mL of CH_2Cl_2. The solution is filtered, and 0.070 g (0.48 mmol) of $(Et_4N)BH_4$ is added with stirring. The product precipitates out of solution and is isolated by filtration. Attempts to recrystallize the product lead to decomposition. Satisfactory elemental analysis could not be obtained for this compound. The purity was determined by the absence of any components of the $[Cl_2FeS_2WS_2]^{2-}$ decomposition product, in the visible spectrum.

Table I. Crystal and Refinement Data for the $[(C_6H_5)_4P]_2[Cl_2FeS_2MS_2FeCl_2]$ Complexes

	M = Mo	M = W
fw		1244.3
a, Å	10.197 (2)	10.215 (6)
b, Å	13.054 (2)	13.071 (5)
c, Å	20.164 (3)	20.187 (7)
α, deg	100.46 (2)	100.54 (3)
β, deg	100.61 (1)	100.58 (2)
γ, deg	100.92 (1)	100.97 (2)
V, Å^3	2524.4	2534.2
space group	$P\bar{1}$	P1
Z	2	2
d_{calcd}, g/cm^3	1.52	1.63
d_{obsd},[a] g/cm^3	1.50 (2)[a]	1.61 (2)[d]
cryst dimens, mm	0.055 × 0.08 × 0.017	0.072 × 0.30 × 0.34
μ, cm^{-1}	12.74	34.41
abs cor (min; max)	1.134; 1.219	1.266; 2.656
$2\theta_{max}$, deg	50	60
no. of unique reflcns	8965	9711
no. of reflcns used ($F^2 > 3\sigma(F^2)$)	5125	9711
parameters	550	550
R[b]	0.058	0.050
R_w[c]	0.072	0.064

[a] By flotation in a CCl_4-pentane mixture. [b] $R = \Sigma||\Delta F|/\Sigma|F_o|$. [c] $R_w = [\Sigma w(\Delta F)^2/\Sigma w|F_o|^2]^{1/2}$. [d] By flotation in a CBr_4-CCl_4 mixture.

X-ray Diffraction Measurements and Collection and Reduction of Data. Details concerning crystal characteristics and X-ray diffraction methodology are shown in Table I. Intensity data were obtained on a Picker-Nuclear four-circle diffractometer equipped with a scintillation counter and pulse-height analyzer and automated by a DEC-PDP8 computer. Graphite-monochromatized Mo Kα radiation ($2\theta_m$ = 12.50°) was used for data collection and cell dimension measurements (Kα$_1$, λ = 0.709 26 Å). Intensity data were collected by using a θ–2θ step scan technique.[20] The basic scan step of 0.10° in 2θ was adjusted with the angle to allow for α_1–α_2 separation at higher angles. Background measurements, 4 s at each end, were made at ±10 steps from the peak maximum. Three standard reflections ($\bar{5}05$; 050; 0,0,$\bar{10}$ for both structures) were measured every 60 data measurements to monitor crystal quality. No crystal decay was observed for either of the two crystals.

The raw data were reduced to net intensities, estimated standard deviations were calculated on the basis of counting statistics, Lorentz polarization corrections were applied, and equivalent reflections were averaged. The estimated standard deviation of the structure factor was taken as the larger of that derived from counting statistics and that derived from the scatter of multiple measurements.

The least-squares program used minimizes $\sum w(\Delta|F|)^2$. The weighting function used throughout the refinements of the structures gives zero weight to those reflections with $F^2 < 3\sigma(F^2)$, and $w = 1/\sigma^2(F)$ to all others [$\sigma^2(F^2) = (0.06F^2)^2 + \sigma^2(F^2)$ (from counting statistics)].[21]

The scattering factors of the neutral non-hydrogen atoms were taken from the tables of Doyle and Turner,[22] and real and imaginary dispersion corrections[23] were applied to all of them. The spherical hydrogen scattering factor tables of Stewart, Davidson, and Simpson[24] were used. Absorption corrections were applied by using the analytical

(20) Baenziger, N. C.; Foster, B. A.; Howells, M.; Howells, R.; Vander Valk, P.; Burton, D. J. *Acta Crystallogr., Sect. B* **1977**, *B33*, 2327.
(21) Grant, D. F.; Killean, R. C. G.; Lawrence, J. L. *Acta Crystallogr., Sect. B* **1969**, *B25*, 374.
(22) Doyle, P. A.; Turner, P. S. *Acta Crystallogr., Sect. A* **1968**, *A24*, 390.
(23) Cromer, D. T.; Liberman, D. *J. Chem. Phys.* **1970**, *53*, 1891.
(24) Stewart, R. F.; Davidson, E. R.; Simpson, W. T. *J. Chem. Phys.* **1965**, *42*, 3175.

Table II. Positional Parameters and Their Standard Deviations in the $[Cl_2FeS_2MoS_2FeCl_2]^{2-}$ Anion

atom	x	y	z
Mo	0.20608 (8)	0.05141 (6)	0.23968 (4)
Fe(1)	0.1434 (1)	−0.0779 (1)	0.32963 (6)
Fe(2)	0.2678 (1)	0.1829 (1)	0.15015 (7)
S(1)	0.3509 (2)	−0.0140 (2)	0.3059 (1)
S(2)	0.0007 (3)	−0.0089 (2)	0.2566 (1)
S(3)	0.2081 (3)	−0.0003 (2)	0.1294 (1)
S(4)	0.2648 (3)	0.2281 (2)	0.2654 (1)
Cl(1)	0.0907 (3)	−0.2575 (2)	0.3090 (1)
Cl(2)	0.1495 (3)	−0.0115 (2)	0.4396 (1)
Cl(3)	0.1212 (3)	0.2601 (3)	0.0930 (1)
Cl(4)	0.4753 (3)	0.2279 (2)	0.1292 (2)

Table III. Positional Parameters and Their Standard Deviations in the $[Cl_2FeS_2WS_2FeCl_2]^{2-}$ Anion

atom	x	y	z
W	0.20628 (3)	0.05109 (2)	0.23933 (1)
Fe(1)	0.1437 (1)	−0.07891 (7)	0.33011 (5)
Fe(2)	0.2677 (1)	0.18376 (8)	0.14902 (5)
S(1)	0.3517 (2)	−0.0137 (2)	0.3053 (1)
S(2)	0.0011 (2)	−0.0092 (2)	0.2564 (1)
S(3)	0.2088 (2)	−0.0014 (1)	0.12933 (9)
S(4)	0.2644 (2)	0.2284 (1)	0.2656 (1)
Cl(1)	0.0913 (3)	−0.2589 (1)	0.3089 (1)
Cl(2)	0.1511 (3)	−0.0109 (1)	0.44032 (9)
Cl(3)	0.1195 (2)	0.2605 (2)	0.0927 (1)
Cl(4)	0.4762 (2)	0.2281 (2)	0.1288 (1)

program ABSORB,[25] which uses the method of de Meulenaer and Tompa.[26]

$(Ph_4P)_2(Cl_2FeS_2MoS_2FeCl_2)$. Crystals suitable for X-ray diffraction work were obtained in a N_2 atmosphere by the slow diffusion of diethyl ether into a CH_2Cl_2 solution of $(Ph_4P)_2(Cl_2FeS_2MoS_2FeCl_2)$. A crystal was lodged into a quartz capillary tube in an inert atmosphere, and the capillary was sealed. This crystal was used for cell dimension measurements and data collection. The cell dimensions (Table I) were obtained by least-squares refinement on the 2θ values of 15 carefully entered reflections with 2θ between 30 and 45°.

$(Ph_4P)_2(Cl_2FeS_2WS_2FeCl_2)$. Single crystals of this complex were obtained in a N_2 atmosphere by the slow diffusion of diethyl ether into a CH_3CN solution of $(Ph_4P)_2(Cl_2FeS_2WS_2FeCl_2)$. The yellow crystals that were found X-ray isomorphous to crystals of the analogous Mo complex were prepared for data collection as described previously for the Mo complex. The cell dimensions (Table I) were obtained as described for the Mo complex.

Determination of the Structures. $(Ph_4P)_2(Cl_2FeS_2MoS_2FeCl_2)$. The structure was solved by conventional Patterson and Fourier techniques and refined by full-matrix least-squares calculations. All atoms in the anion and the two phosphorus atoms were refined with anisotropic temperature factors. The carbon atoms in the cations were refined with isotropic temperature factors. The hydrogen atoms were included in the structure factor calculation at their calculated positions (C–H = 0.95 Å) but were not refined. Refinement converged with final values for R and R_w of 0.065 and 0.081, respectively.

$(Ph_4P)_2(Cl_2FeS_2WS_2FeCl_2)$. The final coordinates from the Mo compound were input for refinement of the data from the W analogue. Refinement under conditions identical with those employed for the Mo complex converged with $R = 0.060$ and $R_w = 0.077$. At this point the carbon atoms of the cations were assigned anisotropic temperature factors. Refinement converged to $R = 0.058$ and $R_w = 0.072$. Incorporation of the hydrogen atoms *fixed* at their calculated positions and further refinement of the rest of the atoms converged to final R and R_w values of 0.050 and 0.064, respectively.

Crystallographic Results. The final atomic positional parameters with standard deviations derived as described previously are compiled in Tables II and III for the $[Cl_2FeS_2MoS_2FeCl_2]^{2-}$ and $[Cl_2FeS_2WS_2FeCl_2]^{2-}$ anions, respectively. Intramolecular distances and angles for both anions are given in Table IV.

(25) Templeton, L.; Templeton, D. "ABSORB"; American Crystallographic Association Meeting: Storrs, CT, 1973; Abstract E10, p 143 (modified for local use by F. J. Hollander).
(26) de Meulenaer, J.; Tompa, H. *Acta Crystallogr.* **1965**, *19*, 1014.

Table IV. Intramolecular Bond Distances (Å) and Angles (deg) in the $[(Cl_2Fe)S_2MS_2(FeCl_2)]^{2-}$ Anions[a]

	$[(Cl_2Fe)S_2MoS_2(FeCl_2)]^{2-}$	$[(Cl_2Fe)S_2WS_2(FeCl_2)]^{2-}$
	Distances	
Fe(1)-Fe(2)	5.552 (2)	5.603 (1)
Fe(1)-Mo(W)	2.771 (2)	2.795 (1)
Fe(2)-Mo(W)	2.781 (2)	2.808 (1)
Mo(W)-S(1)	2.205 (3)	2.205 (2)
Mo(W)-S(2)	2.203 (3)	2.207 (2)
Mo(W)-S(3)	2.208 (3)	2.207 (2)
Mo(W)-S(4)	2.208 (3)	2.217 (2)
Fe(1)-S(1)	2.291 (3)	2.312 (2)
Fe(1)-S(2)	2.300 (3)	2.318 (2)
Fe(2)-S(3)	2.293 (3)	2.321 (2)
Fe(2)-S(4)	2.299 (3)	2.327 (2)
Fe(1)-Cl(1)	2.246 (3)	2.252 (2)
Fe(1)-Cl(2)	2.215 (3)	2.221 (2)
Fe(2)-Cl(3)	2.221 (3)	2.226 (2)
Fe(2)-Cl(4)	2.225 (3)	2.231 (2)
S(1)-S(2)	3.543 (4)	3.551 (3)
S(3)-S(4)	3.541 (4)	3.559 (3)
S(1)-S(3)	3.639 (5)	3.629 (3)
S(1)-S(4)	3.627 (4)	3.631 (3)
S(2)-S(4)	3.649 (5)	3.653 (3)
S(2)-S(3)	3.615 (4)	3.620 (3)
Cl(1)-Cl(2)	3.636 (4)	3.664 (3)
Cl(3)-Cl(4)	3.669 (5)	3.703 (3)
Cl(1)-S(2)	3.809 (5)	3.830 (3)
Cl(1)-S(1)	3.752 (5)	3.777 (3)
Cl(2)-S(1)	3.677 (5)	3.697 (3)
Cl(2)-S(2)	3.732 (5)	3.754 (3)
Cl(3)-S(3)	3.833 (5)	3.869 (3)
Cl(3)-S(4)	3.645 (5)	3.663 (3)
Cl(4)-S(3)	3.638 (5)	3.656 (3)
Cl(4)-S(4)	3.785 (5)	3.809 (3)
	Angles	
Fe(1)-Mo(W)-Fe(2)	179.37 (6)	179.25 (4)
S(1)-Mo(W)-S(2)	106.98 (13)	107.19 (10)
S(1)-Mo(W)-S(3)	111.09 (13)	110.66 (10)
S(1)-Mo(W)-S(4)	110.55 (14)	110.40 (11)
S(2)-Mo(W)-S(3)	110.04 (14)	110.18 (11)
S(2)-Mo(W)-S(4)	111.64 (14)	111.33 (11)
S(3)-Mo(W)-S(4)	106.60 (13)	107.10 (10)
S(1)-Fe(1)-S(2)	101.03 (13)	100.14 (10)
S(1)-Fe(1)-Cl(1)	111.61 (13)	111.66 (10)
S(1)-Fe(1)-Cl(2)	109.37 (14)	109.24 (11)
S(2)-Fe(1)-Cl(1)	113.84 (14)	113.88 (12)
S(2)-Fe(1)-Cl(2)	111.51 (14)	111.55 (11)
Cl(1)-Fe(1)-Cl(2)	109.23 (14)	109.98 (11)
S(3)-Fe(2)-S(4)	100.91 (12)	99.95 (9)
S(3)-Fe(2)-Cl(3)	116.18 (15)	116.64 (12)
S(3)-Fe(2)-Cl(4)	107.27 (14)	106.88 (11)
S(4)-Fe(2)-Cl(3)	107.47 (13)	107.15 (11)
S(4)-Fe(2)-Cl(4)	113.57 (15)	113.35 (11)
Cl(3)-Fe(2)-Cl(4)	111.20 (16)	112.40 (13)
Fe(1)-S(1)-Mo(W)	76.05 (8)	76.40 (6)
Fe(1)-S(2)-Mo(W)	75.91 (8)	76.24 (6)
Fe(2)-S(3)-Mo(W)	76.29 (8)	76.62 (6)
Fe(2)-S(4)-Mo(W)	76.19 (8)	76.32 (6)

[a] The structural parameters for the counterions in the complexes are unexceptional. Thus, for the two independent cations in $[(C_6H_5)_4P]_2[Cl_2FeS_2MoS_2FeCl_2]$ the eight P–C bonds are within the range of 1.781 (8)–1.823 (8) Å with a mean value of 1.798 (13) Å. The C–C bonds are within the range of 1.326 (16)–1.410 (12) Å with a mean value of 1.377 (19) Å. The 12 C_i–P–C_j angles are found between 106.3 (5) and 111.9 (5)° with a mean value of 109.5 (2.0)°. For the cation in the structure of $[(C_6H_5)_4P]_2[Cl_2FeS_2WS_2FeCl_2]$ the P–C bonds are in the range of 1.786 (6)–1.810 (7) Å with a mean value of 1.794 (9) Å. The C_i–P–C_j angles are found between 106.8 (4) and 112.4 (4)° with a mean value of 109.5 (2.0)°. The 48 C–C bonds are within the range of 1.340 (13)–1.404 (11) Å with a mean value of 1.380 (11) Å. In all cases the standard deviations from the mean have been obtained as follows: $\sigma = S = [\sum_{i=1}^{N}(X_i - \bar{X})^2/N - 1]^{1/2}$ where X_i is the value of an individual bond or angle and $\bar{X}$ is the mean value for the N equivalent bond lengths or angles.

Table V. Electronic Spectra of the Fe–M–S Complexes (M = Mo, W)

complex	solvent	λ_{max}, nm (ϵ, M^{-1} cm^{-1}) region A	region B	region C	other
$[Cl_2FeS_2MoS_2FeCl_2]^{2-}$	CH_2Cl_2	1038 br 960 (390)	600 (580) 566 sh	475 (9890) 398 (4369)	319 (13 870)
	DMF	1085 (130)	600 sh 522 sh	472 (5850) 432 (4070)	314 (12 250)
$[Cl_2FeS_2WS_2FeCl_2]^{2-}$	CH_2Cl_2	1050 (400)	502 (930)	418 (7100) 360 (5400)	294 (14 200)
	DMF	1150 (460)	524 (530)	417 (6300) 373 (7110)	
$[(MoS_4Fe_2Cl_3)^{2-}]_x$	DMF		580 (4410)	530 (5680) 432 (5380)	
$[(WS_4Fe_2Cl_3)^{2-}]_x$	DMF		555 sh 510 (8790) 430 (8550)	414 (8720) 346 (9110)	

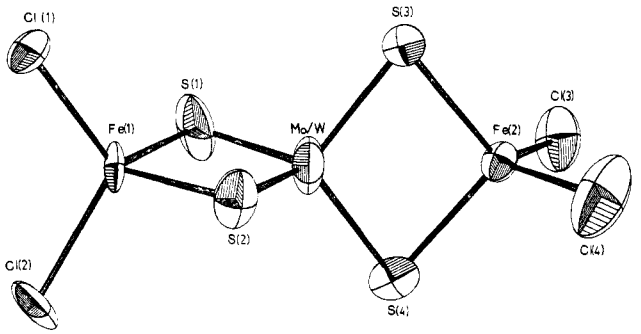

Figure 2. Atom-labeling and -numbering scheme of the $[Cl_2FeS_2MS_2FeCl_2]^{2-}$ anions (M = Mo, W). Thermal ellipsoids as drawn by ORTEP[51] represent the 50% probability surfaces.

The atom-labeling scheme is shown in Figure 2. Deposited with the microfilm version of the journal are (a) tables of the observed values of F, their esd's, and the $|F_o| - |F_c|$ values for both structures, (b) the final atomic positional and thermal parameters for the phosphorus and carbon atoms of the cations in both structures, (c) the final atomic positional and thermal parameters of the hydrogen atoms in both structures, and (d) a stereopair drawing of the unit cell contents.

Results and Discussion

Synthesis. The synthesis of the $[Cl_2FeS_2MS_2FeCl_2]^{2-}$ complexes (M = Mo (I), W (II)) is accomplished readily in excellent yields either by the oxidation of the $[(PhS)_2FeS_2MS_2]^{2-}$ complexes with ferric chloride or directly from $FeCl_2$ and the MS_4^{2-} thioanions. The reaction of the $[(PhS)_2FeS_2MS_2]^{2-}$ complexes with $FeCl_3 \cdot 6H_2O$ in dimethylformamide (DMF) solution results in the oxidation of the PhS^- ligands and the concomitant generation of $FeCl_2$, which subsequently coordinates to the MS_4^{2-} anions (eq 1).

$$[(PhS)_2FeS_2MS_2]^{2-} + 2FeCl_3 \xrightarrow{DMF} [Cl_2FeS_2MS_2FeCl_2]^{2-} + PhSSPh + Fe^{2+} + 2Cl^-$$

The electronic spectra of I and II (Table V) in CH_2Cl_2 solution are different from those observed in DMF solution. It appears that the interactions of the $FeCl_2$ molecules with the MS_4^{2-} centers in either I or II are rather weak and coordinating solvents such as DMF solvolyze the $FeCl_2$ units. The electronic spectra of the $[Cl_2FeS_2MS_2]^{2-}$ complexes in either CH_2Cl_2 or DMF are similar to those of the $[Cl_2FeS_2MS_2FeCl_2]^{2-}$ complexes in DMF and indicate that in DMF the equilibrium

$$[Cl_2FeMS_4]^{2-} + FeCl_2 \underset{}{\overset{Q}{\rightleftharpoons}} [Cl_2FeS_2MS_2FeCl_2]^{2-} \quad (1)$$

is established. The $[Cl_2FeS_2MS_2]^{2-}$ complexes, which were obtained readily in stoichiometric reactions between the MS_4^{2-} anions and $FeCl_2$, react further with $FeCl_2$ in DMF to form I and II. The isolation of I or II from DMF solutions, containing an excess of $FeCl_2$, is accomplished readily by the addition of diethyl ether. The equilibrium constant Q for M = Mo (eq 1) at 298 K in DMF solution is 334 ± 10 M^{-1}.[27] The lability of the MS_4^{2-} anions in I and II as bridging ligands is demonstrated by reaction 2, which proceeds readily in

$$[Cl_2FeS_2MS_2FeCl_2]^{2-} + MS_4^{2-} \rightarrow 2[Cl_2FeS_2MS_2]^{2-} \quad (2)$$

CH_3CN solution. From the reaction of $[(PhS)_2FeS_2WS_2]^{2-}$ with $FeCl_3 \cdot 6H_2O$ in DMF, II can be readily isolated only when it is rapidly precipitated out of solution by the addition of an ethanol–ether mixture. Slow crystallization over ca. 48 h results in the formation of crystals of $[Fe(DMF)_6][Cl_2FeS_2WS_2]$ whose identity has been established by X-ray crystallography.[28]

Both I and II undergo chemical reduction with tetraalkylammonium salts of the BH_4^- anion in either CH_3CN or CH_2Cl_2 solution. The overall stoichiometry of the reaction is

$$(R_4N)_2(Cl_2FeS_2MoS_2FeCl_2) + R_4NBH_4 \rightarrow (R_4N)_2MoS_4Fe_2Cl_3 + R_4NCl + {}^1/_2B_2H_6 + {}^1/_2H_2$$

This stoichiometry has been confirmed by elemental analysis of the reduction product $(R_4N)_2MoS_4Fe_2Cl_3$ (R = Et) and Cl^- analysis of the byproducts. The latter shows that approximately 1 mmol of Cl^- is released/mmol of $(Et_4N)_2(Cl_2FeS_2MoS_2FeCl_2)$.[29] The R_4N^+ salts of $(MoS_4Fe_2Cl_3)^{2-}$ can be isolated in microcrystalline form; however, to date we have been unable to obtain single crystals suitable for an X-ray structure determination.

In *N*-methylformamide (NMF) solution the $[MoS_4Fe_2Cl_3]^{2-}$ anion (I^-) is converted rapidly to the $[Fe(MoS_4)_2]^{3-}$ complex.[17] From this reaction, with use of $(Ph_4P)_2MoS_4Fe_2Cl_3$ known extinction coefficients and on the assumption of quantitative transfer of the MoS_4^{2-} anion to the $[Fe(MoS_4)_2]^{3-}$ complex, a formula weight of 1069 can be calculated for the $(Ph_4P)_2MoS_4Fe_2Cl_3$ complex. This value compares reasonably well with the theoretical formula weight of 1121.

Infrared and Visible Spectra. The infrared spectra of I and II in the solid are distinctly different from those of the $[Cl_2FeS_2MS_2]^{2-}$ complexes, as expected on the basis of symmetry considerations. A raising of the MS_4^{2-} site symmetry from C_{2v} in the $[(L)_2FeS_2MS_2]^{2-}$ complexes to D_{2d} in I and II results in fewer infrared-active vibrations for the highly symmetric bridging ligand. The typical quartet pattern of

(27) The equilibrium constant was determined spectrophotometrically from a plot of E vs. $E - E_0$. From the equation $E = E_\infty - (1/Q)(E - E_0)/[FeCl_2]$ where E_0 and E_∞ are the molar extinction coefficient of $[Cl_2FeMoS_4]^{2-}$ and $[MoS_4(FeCl_2)_2]^{2-}$, respectively, and E is the experimentally observed molar absorptivity. $1/Q$ can be obtained from the slope. The intercept gives E_∞, which at 477 nm is 10 227 M^{-1} cm^{-1}.
(28) Stremple, P.; Coucouvanis, D., manuscript in preparation.
(29) The reduction of $(Bu_4N)_2(Cl_2FeS_2MoS_2FeCl_2)$ by Bu_4NBH_4 was monitored spectrophotometrically. Two isosbestic points were observed showing that there exist no additional intermediates.

absorptions that derive from the bridging and terminal M–S vibrations in the $[(L)_2FeS_2MS_2]^{2-}$ complexes[12,30] is reduced to doublets for the M–S bridging vibrations in the spectrum of I (460 sh, 470 cm^{-1}) and II (468, 458 cm^{-1}). The resonance Raman spectrum of I has been reported,[31] and an enhancement of a vibration at 440 cm^{-1} is observed upon irradiation at 488 nm. The reduction product of I also shows a doublet of absorptions at 465 and 475 cm^{-1} that suggest that in this compound only doubly bridging tetrathiomolybdates are present.

The electronic spectra of the complexes (Table V) in the visible–near-infrared regions are characterized by absorptions that can be separated into three groups.[32] A group of intense absorptions between 300–500 nm, a group of less intense absorptions between 500 and 650 nm, and an envelope of weak absorptions around 1000 nm. The average values of the absorptions in the 300–500-nm region for I and I^- are 436 and 481 cm^{-1}, respectively, and are very close to the energy of the S → Mo ($\pi(t_1) \rightarrow d(e)$) transition in the MoS_4^{2-} anion (475 nm).[33] The absorptions at 418 and 360 nm in II and at 346 and 414 nm in II^- average to 389 and 380 nm, respectively, and compare well with the S → W ($\pi(t_1) \rightarrow d(e)$) transition at 392 nm.

The transitions, found in all complexes, between 650 and 500 nm, tentatively are assigned to the Fe–S chromophores, since no such low-energy transitions are observed in the spectra of the MS_4^{2-} anions. Again, hypsochromic shifts are observed for these bonds in the spectra of the WS_4^{2-} complexes (II and II^-). A unique feature in the near-infrared reflectance and solution electronic spectra of the trimeric MS_4^{2-} complexes is a broad absorption band with considerable structure centered around 1000 nm. We tentatively assigned[32] these envelopes of absorptions to Fe → Mo(W) transitions. The energies of these transitions when compared to the energies of the S → Mo(W) transitions suggest that in the MS_4–Fe complexes the Fe d orbitals are located somewhere between the primarily sulfur molecular orbitals and the empty Mo(VI) or W(VI) d orbitals. Such an ordering of the energy levels also has been advanced on the basis of a semiquantitative calculation.[34]

Structures of the $(Ph_4P)_2Cl_2FeS_2MS_2FeCl_2$ Complexes. The Ph_4P^+ salts of both I and II are X-ray isomorphous and isostructural. The structures show well-separated anions with no unusually short interionic contacts. Important intramolecular distances and angles are shown in Table IV. For both I and II the structure of the anion is best described as a symmetric linear array of three edge-sharing tetrahedra.

In this array the central S_2MS_2 tetrahedral unit is $(\mu\text{-}S)_2$ bridging each of the two terminal Cl_2Fe units. The Fe–M–Fe arrays are nearly linear with angles of 179.37 (6) and 179.25 (4)° for M = Mo and W, respectively. The Fe–Fe distances in I and II are 5.552 (2) and 5.603 (1) Å, respectively. The mean values of the Fe–M distances for I and II at 2.776 (5) and 2.802 (6) Å are somewhat longer than the Fe–M distances in the $[(PhS)_2FeS_2MS_2]^{2-}$ (III) (2.740 (1) and 2.775 (1) Å for M = Mo and W, respectively) and the $[(S_5)FeS_2MS_2]^{2-}$ (IV) anions (2.737 (3) and 2.752 (3) Å for M = Mo and W, respectively).[12b] The weaker Fe–M interactions suggested by these differences also are apparent in differences in the $\overline{Fe–S}$ bond lengths in I and II, which at 2.296 (4) and 2.320 (6) Å, respectively, are slightly longer than the corresponding distances in III and IV.

Table VI. Isomer Shift and Quadrupole Splittings of Fe–M–S Complexes and Representative High-Spin Fe(II) Tetrahedral Complexes

complex	δ	ΔE_Q	ref
$[Cl_2FeS_2MoS_2FeCl_2]^{2-}$	0.57	1.98	this work
$[Cl_2FeS_2WS_2FeCl_2]^{2-}$	0.63	2.14	this work
$[(Cl_2FeS_2MoS_2FeCl)^{2-}]_x$	0.50	1.12	this work
$[Fe(SPh)_4]^{2-}$	0.64	3.24	42
$[Fe(SPh)_2(S_2C_4O_2)]^{2-}$	0.64	2.88	42
$[Fe(SPh)_2S_2MoS_2]^{2-}$	0.44	1.96	12
$[FeCl_4]^{2-}$	0.86	2.61	41

The $\overline{Fe–S_b}$ bonds in III are 2.263 (3) and 2.290 (2) Å for M = Mo and W, and in IV the analogous distances are 2.248 (6) and 2.27 (1) Å. The $\overline{Fe–S–M}$ angles in I and II at 76.1 (2) and 76.4 (2)°, respectively, are somewhat larger than the corresponding angles in III (74.5 (3), 75.4 (3)°) and IV (74.7 (2), 74.9 (4)°). The $\overline{M–S}$ bond lengths in I and II at 2.206 (2) and 2.209 (5) Å are longer than the $\overline{M–S}$ bonds in $(Et_4N)_2MoS_4$[35] (2.177 (6) Å) and $(NH_4)_2WS_4$[36] (2.17 (1) Å).

The S_2MS_2 units in I and II do not deviate appreciably from tetrahedral geometry, and the 12 independent S–M–S angles range from 106.6 (1) to 111.6 (1)°. By comparison, a wider range in the tetrahedral angles around the iron atoms is observed, and the smaller S_b–Fe–S_b angles are found within the FeS_2M rhombic units (101.0 (1) and 100.1 (1)°, respectively, for M = Mo and W). The corresponding S_b–Fe–S_b angles in III (105.42 (9) and 102.96 (9)° for M = Mo and W, respectively) and in IV (105.5 (3) and 104.7 (3) for M = Mo and W, respectively) are somewhat larger. Collectively the values of the Fe–M distances, the Fe–S_b–M angles, the Fe–S bond lengths, and the S_b–Fe–S_b angles in I and II (by comparison to III and IV) reveal that the S_2MS_2 anions are weaker ligands in the doubly bridging mode. The longer M–S bond lengths in the MS_4 units of I and II by comparison to the $\overline{M–S}$ bonds in the free MS_4^{2-} anions suggest that there exists some electron delocalization from the iron atoms toward the Mo and W atoms and a partial reduction of the latter. A comparison of the structural details between I and II, and particularly the slightly longer W–Fe and Fe–S distances in II, suggest weaker Fe–S_2MS_2–Fe interactions for M = W. A comparison between the bond lengths in the first and second coordination spheres around the Mo atom in I and corresponding structural data available for the Mo site in nitrogenase show some similarities and some differences. It appears that the number of iron and sulfur atom around the molybdenum atom in I are comparable to the numbers obtained for the Mo site in nitrogenase by EXAFS analyses.[3,37] An examination of the EXAFS data, however, shows appreciably longer $\overline{Mo–S}$ bonds in the Mo site of nitrogenase (2.35 Å) by comparison to the $\overline{Mo–S}$ bond in I (2.207 Å). This significant difference could be attributed to differences in the Mo formal oxidation states between I and the Mo site in nitrogenase. The longer Mo–S bonds in the latter compare favorably with the $\overline{Mo–S}$ bonds in the "Fe_3Mo" cubanes[10,11] in which the formal oxidation state of the Mo atoms is between 3+ and 4+. Similarly, the $\overline{Mo–S}$

(30) Paulat-Böschen, I.; Krebs, B.; Müller, A.; Koniger-Ahlborn, E.; Dornfeld, H.; Schultz, H. *Inorg. Chem.* **1978**, *17*, 1440.
(31) Müller, A.; Sarkar, S.; Dammrose, A.; Filgueira, R. *Z. Naturforsch., B: Anorg. Chem., Org. Chem.* **1980**, *35B*, 1592–1593.
(32) Coucouvanis, D. *Acc. Chem. Res.* **1981**, *14*, 201–209 and references therein.
(33) Stiefel, E. I. *Prog. Inorg. Chem.* **1977**, *22*, 1.
(34) Müller, A.; Jostes, R.; Tölle, H. G.; Trautwein, A.; Bill, E. *Inorg. Chim. Acta* **1980**, *46*, L121.
(35) (a) Koz'min, D. A.; Popova, Z. V. *Zh. Strukt. Khim.* **1971**, *12*, 99. (b) Kanatzidis, M. G.; Coucouvanis, D. *Acta Crystallogr., Sect. C: Cryst. Struct. Commun.* **1983**, *C39*, 835–838.
(36) Sasvari, K. *Acta Crystallogr.* **1963**, *16*, 719.
(37) A recent determination of the metal and sulfur composition of the iron–molybdenum cofactor of nitrogenase has led to an updated Mo/Fe/S stoichiometry of 1/6/8 or 9: Nelson, M. J.; Levy, M. A.; Orme-Johnson, W. H. *Proc. Natl. Acad. Sci. U.S.A.* **1983**, *80*, 147. This determination is more in accord with recent Fe EXAFS results that indicate three to four S(Cl) neighbors around the iron atoms: Antonio, M. R.; Teo, B. K.; Orme-Johnson, W. H.; Nelson, M. J.; Groh, S. E.; Lindahl, P. A.; Kauzlarich, S. M.; Averill, B. A. *J. Am. Chem. Soc.* **1982**, *104*, 4703.

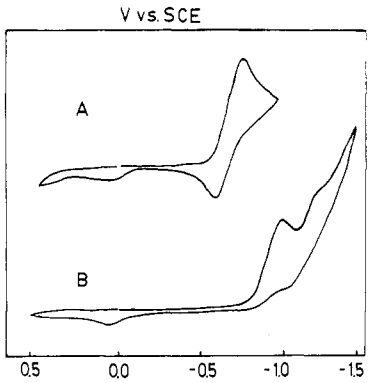

Figure 3. Cyclic voltammograms for $[Cl_2FeS_2MoS_2FeCl_2]^{2-}$ (A) and $[Cl_2FeS_2WS_2FeCl_2]^{2-}$ (B) (platinum-bead electrode; 3×10^{-3} M in CH_2Cl_2 solution; vs. SCE).

bond distance in MoS_9^{2-}, which formally contains Mo(IV), is 2.359.[38]

A common structural feature of the Fe–Mo–S complexes that contain the FeS_2Mo rhombic units is the rather short Fe–Mo distance of 2.7 ± 0.1 Å. The location of iron atoms at a similar distance from the molybdenum in nitrogenase strongly suggests that the FeS_2Mo rhombic unit, which is a common feature in the two proposed models for th Mo coordination environment, also is a structural feature of the nitrogenase active site.

Mössbauer Spectra and Magnetic Properties. The Mössbauer spectra of I and II[39] (Table VI) are similar and show one quadrupole doublet for each of the complexes. The quadrupole splitting is practically constant between 4.2 and 300 K for both I and II. The data indicate that the E_g orbital states of a d^6 configuration, lying lowest in tetrahedral coordination, are split by more than 500 cm^{-1}. This behavior is a common feature in most complexes with a tetrahedral FeS_4 unit.[40] Application of an external magnetic field of 0.9 T at 4.2 K has no effect on the spectrum of the Mo complex other than a small line broadening expected for a diamagnetic complex. By contrast, the spectrum of the W homologue shows significant magnetic hyperfine splitting.[39] The diamagnetic behavior of I suggests antiferromagnetic coupling between the $S = 2$ iron ions, which results in a $S = 0$ ground state. The magnetic splitting observed in the W complex indicates that the coupling in this complex is weaker than that of the Mo complex. This difference in the antiferromagnetic coupling between I and II, which also is apparent in magnetic susceptibility measurements,[39] may be a consequence of the small differences in the structures of I and II. These structural parameters (longer Fe–Fe, Fe–S_b, and Fe–W bond length in II) show a weaker MS_4 bridge in II and may be correlated with the difference in the antiferromagnetic coupling constants.

The isomer shifts of I and II (Table VI) are lower than those expected for a tetrahedral Cl_2FeS_2 unit by comparison to isomer shift values for the $(FeCl_4)^{2-}$[41] and $[Fe(SPh)_4]^{2-}$[42] anions (Table VI). Although the correlation of valence state and isomer shift is complicated, it is firmly established[43] that a decrease in the population of d orbitals results in a decrease in isomer shift.

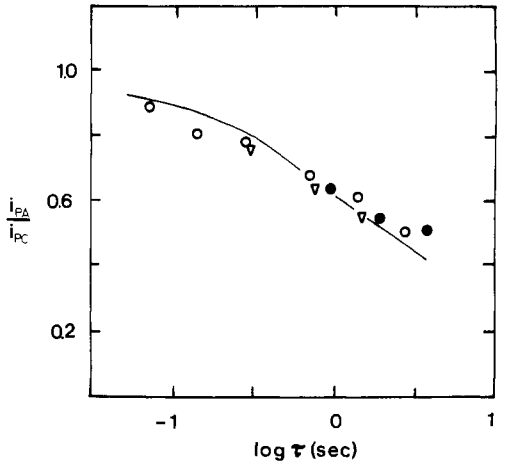

Figure 4. Peak current ratios for the reduction of $[Cl_2FeS_2MoS_2FeCl_2]^{2-}$ in CH_2Cl_2. The line is the theoretical line for $k_f = 0.5$ s^{-1}, and τ is the time between the $E°$ and the switching potential. Concentrations are as follows: ●, 0.94 mM; ○, 0.57 mM; ▽, 0.31 mM.

The smaller values of the isomer shift in I and II give additional support to previous arguments[32,44] that the MS_4^{2-} (M = Mo, W) anions act as charge-delocalizing ligands by means of low-lying vacant metal d orbitals. Just as observed previously for the $[(PhS)_2FeS_2MS_2]^{2-}$ complexes,[12] the isomer shift value of the iron atoms in the $[Cl_2FeS_2MS_2FeCl_2]$ complexes is greater for the W complex and reflects less electron delocalization to the WS_4^{2-} unit.

The Mössbauer spectrum of I^- shows one quadrupole doublet (Table VI) with an isomer shift even smaller than that of I. This behavior can only be explained if one assumes that the reduction is centered on the molybdenum atom.

Redox Chemistry of the $[Cl_2FeS_2MS_2FeCl_2]^{2-}$ Complexes. The electrochemical reduction of I in CH_2Cl_2 solution (Figure 3) is apparent in a single one-electron wave with $E_{1/2}$ of −0.56 V vs. SCE. Cyclic voltammetric measurements show the reduction product to be unstable and to undergo a slow irreversible first-order chemical reaction. A plot of i_{pa}/i_{pc} vs. log τ (Figure 4) for various concentrations and two different counterions (Ph_4P^+, Bu_4N^+) shows i_{pa}/i_{pc} essentially independent of concentration and suggests that the reaction following electron transfer is first order in I and not a coupling reaction. The theoretical line for a possible EC mechanism (Scheme I) is also shown in Figure 4 for a rate constant of

Scheme I

$$[Cl_2FeS_2MoS_2FeCl_2]^{2-} + e^- \rightarrow$$

$$[Cl_2FeS_2MoS_2FeCl_2]^{3-} \xrightarrow{k} [(MoS_4)Fe_2Cl_3]^{2-} + Cl^-$$

0.5 s^{-1}. The rather significant deviations from this line suggest that the mechanism is more complicated than the simple EC mechanism shown above. Possible complications may arise by the presence of the Cl^- product that could inhibit the loss of Cl^- from (I^-) or interact with I. An attempt to study the effects of excess Cl^- in the reduction of I was hindered by the reaction

$$[Cl_2FeS_2MoS_2FeCl_2]^{2-} + 2Cl^- \rightleftarrows FeCl_4^{2-} + [Cl_2FeS_2MoS_2]^{2-}$$

Some typical data for the cyclic voltammetry and chronoam-

(38) Draganjac, M.; Simhon, E.; Chan, L. T.; Kanatzidis, M.; Baenziger, N. C.; Coucouvanis, D. *Inorg. Chem.* **1982**, *21*, 3321.
(39) Simopoulos, A.; Papaefthymiou, V.; Kostikas, A.; Petrouleas, V.; Coucouvanis, D.; Simhon, E. D.; Stremple, P. *Chem. Phys. Lett.* **1981**, *81*, 261.
(40) Kostikas, A.; Petrouleas, V.; Simopoulos, A.; Coucouvanis, D.; Holah, D. G. *Chem. Phys. Lett.* **1976**, *38*, 582.
(41) Edwards, P. R.; Johnson, C. E.; Williams, R. S. P. *J. Chem. Phys.* **1967** *47*, 2074.
(42) Coucouvanis, D.; Swenson, D.; Baenziger, N. C.; Murphy, C.; Holah, D. G.; Sfarnas, N.; Simopoulos, A.; Kostikas, A. *J. Am. Chem. Soc.* **1981**, *103*, 3350–3362.
(43) Walker, L. R.; Wertheim, G. K.; Jaccarino, V. *Phys. Rev. Lett.* **1961**, *6*, 98.
(44) Müller, A.; Jostes, R.; Flemming, V.; Potthast, R. *Inorg. Chim. Acta* **1980**, *44*, L33.

Table VII. Cyclic Voltammetric Data

υ, V/s	E_{pc}, V vs. SCE	i_{pc}, μA	$i_{pc}/\upsilon^{1/2}C$, μA/((V/s)$^{1/2}$ mM)	E_{pa}	i_{pa}/i_{pc}
A. $(Bu_4N)_2(Cl_2FeS_2MoS_2FeCl_2)$[a,b]					
0.02	−0.585	1.75	21.7		
0.05	−0.590	2.5	19.6	−0.505	0.51
0.10	−0.591	3.3	18.3	−0.505	0.62
0.20	−0.599	4.5	17.6	−0.505	0.68
B. $(Ph_4P)_2(Br_2FeS_2MoS_2FeBr_2$[b,c]					
0.05	−0.550	3.2	16.6		
0.10	−0.560	4.2	15.4	−0.420	
0.20	−0.560	5.9	15.3	−0.480	0.47
0.50	−0.566	11.2	18.4	−0.480	0.54
1.0	−0.575	14	16.3	−0.490	0.50
2.0	−0.584	17	14.0	−0.48	0.70
5.0	−0.594	24	12.5[d]	−0.456	0.80
C. $[(Et_4N)_2MoS_4Fe_2Cl_3]_x$[e,f]					
0.020	−0.90	5.5	11.3		
	−1.205	9.8	20.1		
0.050	−0.90	7.8	10.1		
	−1.444	14	18.2		
0.100	−0.91	10.5	9.7		
	−1.23	19	17.4		
0.200	−0.95	16.5	10.7		
	−1.27	28	18.2		
D. $(Ph_4P)_2(Cl_2FeS_2WS_2FeCl_2)$[b,g]					
0.05	−0.81	3.8	17.2		
0.10	−0.83	5.3	17.2		
0.20	−0.84	7.7	17.5		
0.50	−0.85	11	15.7		

[a] 1.02 mM $(Bu_4N)_2(Cl_2FeS_2MoS_2FeCl_2)$; 0.10 M Bu_4NClO_4 in CH_2Cl_2; hanging-mercury-drop electrode (HMDE); 298 ± 3 K. [b] The values of $i_{pc}/\upsilon^{1/2}C$ obtained for the known one-electron reduction of $[Fe_4S_4(SPh)_4]^{2-}$ in DMF (corrected for viscocity) fall in the range 16–20 μA/(V/s)$^{1/2}$ mM. [c] 0.86 mM $(Ph_4P)_2(Br_2FeS_2MoS_2FeBr_2)$; 0.113 M Bu_4NClO_4 in CH_2Cl_2; HMDE; 298 ± 3 K. [d] The apparent drop in the current function from 21.7 to 12.5 μA/(V/s)$^{1/2}$ mM is attributed to the quasi-reversibility of the electron-transfer process. A better measure of diffusion control is the $i\tau^{1/2}/C$ function from chronoamperometry (see Table VIII) where the electron-transfer rate has been eliminated. [e] 3.44 mM $(Et_4N)_2MoS_4Fe_2Cl_3$; 0.10 M Bu_4NClO_4 in DMF; Pt electrode; 298 ± 3 K. [f] The values of $i_{pc}/\upsilon^{1/2}C$ obtained for the known one-electron oxidation of $[Ni(S_2C_2(CN)_2)]^{2-}$ in DMF and for the one-electron oxidation of $[Cu(S_2C_2O_2)_2]^{2-}$ in CH_2Cl_2 (corrected for viscocity) fall in the range 35–40 μA/(V/s)$^{1/2}$ mM. [g] 0.99 mM $(Ph_4P)_2(Cl_2FeS_2WS_2FeCl_2)$; 0.10 M Bu_4NClO_4 in CH_2Cl_2; HMDE; 298 ± 3 K. Two additional cathodic waves were observed at 1.05 and −1.20 V at a scan rate of 0.20 V/s.

perometry measurements on $(Bu_4N)_2Cl_2FeS_2MoS_2FeCl_2$ are shown in Tables VII and VIII. These data were obtained by using a hanging-mercury-drop electrode (HMDE) as the working electrode.[45] The current functions are all consistent with a diffusion-controlled one-electron reduction. The peak current ratios in cyclic voltammetry and the current ratios in chromoamperometry demonstrate the instability of the initial reduction product. The data for $(Ph_4P)_2Br_2FeS_2MoS_2FeBr_2$ (Table VII) are similar. The smaller i_a/i_c peak current ratios for the bromo derivative suggest a faster decomposition for the reduction product of the latter. The electrochemistry of the final reduction product $(Et_4N)_2MoS_4Fe_2Cl_3$ in DMF shows two small reduction waves and a single oxidation wave around +0.08 V vs. SCE. The oxidation wave was accompanied by considerable electrode filming and was not studied any further. The first reduction wave at −0.90 V vs. SCE has a current function of 10 μA/(V/s)$^{1/2}$ mM. The second wave at −1.21 V vs. SCE has a total current function of 18 μA/(V/s)$^{1/2}$ mM.

(45) Filming did not present a problem on the HMDE as evidenced by the constancy of the $i\tau^{1/2}$ values in chronoamperometry (Table VIII).

Table VIII. Chronoamperometric Data

τ, s	i_c, μA	i_a/i_c	$i_c\tau^{1/2}/C$, μA s$^{1/2}$/mM
A. $(Bu_4N)_2(Cl_2FeS_2MoS_2FeCl_2)$[a,b]			
0.05	12.2	0.26	2.73
0.10	8.7	0.22	2.74
0.20	6.5	0.22	2.91
0.50	4.2	0.19	2.97
1.0	3.0	0.15	2.99
2.0	1.7	0.13	2.39
B. $(Et_4N)_2(MoS_4Fe_2Cl_3)$[c,d]			
0.020	140	0.21	5.76
0.050	88	0.17	5.72
0.10	61	0.15	5.61
0.20	48	0.04	6.24
0.50	32		6.58
1.00	25.5		7.41

[a] 0.57 mM $(Bu_4N)_2(Cl_2FeS_2MoS_2FeCl_2)$; 0.10 M Bu_4NClO_4 in CH_2Cl_2; HMDE; 298 ± 3 K. [b] The values of $i\tau^{1/2}/C$ calculated for the one-electron reduction of $[Fe_4S_4(SPh)_4]^{2-}$ in DMF (corrected for viscocity) fall in the range 2.8–3.5 μA s$^{1/2}$/mM. [c] 3.44 mM $(Et_4N)_2MoS_4Fe_2Cl_3$; 0.10 M Bu_4NClO_4 in DMF; Pt electrode; 298 ± 3 K. E_{in} = −0.5 V; E_f = 1.4 V. [d] For the reduction of $[Fe_4S_4(SPh)_4]^{2-}$ in DMF (n = 1), $i\tau^{1/2}/C$ = 10–12.

Under the assumption that the reduction product (I^-) is pure,[46] these values for the current functions are considerably smaller than the value of 35–40 μA/(V/s)$^{1/2}$ mM expected for a one-electron diffusion-controlled process (Table VII, footnote *f*) and suggest that the reduction waves correspond to 0.5 electron/$[MoS_4Fe_2Cl_3]^{2-}$ unit or one electron for a $[(MoS_4Fe_2Cl_3)_2]^{4-}$ dimer.[47] The chronoamperometric analysis results (Table VIII) of the $([MoS_4Fe_2Cl_3]^{2-})_x$ product also show small values for the current function (5.7 μA s$^{1/2}$/mM) if the product is assumed to be monomeric $[MoS_4Fe_2Cl_3]^{2-}$. The expected value[48] of the current function for a one-electron diffusion-controlled process in chronoamperometry is 10–12 μA s$^{1/2}$/mM. Such a value can be obtained if the $[MoS_4Fe_2Cl_3]^{2-}$ product exists as a dimer in solution. The electrochemistry of the Bu_4N^+ salt of the $([MoS_4Fe_2Cl_3]^{2-})_x$ reduction product gave essentially the same results.[49]

The coulometric reduction of $(Ph_4P)_2(Cl_2FeS_2MoS_2FeCl_2)$ on a Pt electrode was complicated by electrode filming, which substantially lowered the current and increased the electrolysis time to several hours. As a result, it was difficult to calculate the coulometric n value because of the uncertainty in the residual current. The electronic spectrum of the coulometrically reduced product however was identical with the spectrum of $([MoS_4Fe_2Cl_3]^{2-})_x$ obtained by borohydride reduction.

The voltammetric reduction of $(Ph_4P)_2Cl_2FeS_2WS_2FeCl_2$ was examined on both a HMDE and a platinum electrode. On platinum, filming was so extreme that no waves were observed unless the electrode was cleaned after every scan. On the HMDE, good waves could be seen, as a new surface was obtained for each scan. Three irreversible reduction waves were obtained at −0.84, −1.05, and −1.20 V vs. SCE (Table

(46) The extreme sensitivity of $[(MoS_4)Fe_2Cl_3]_2^{4-}$ toward oxidation and failure in obtaining this material in high crystalline form make it difficult to ascertain its purity. However, as the analytical results indicate, only a small amount of impurity may be present.

(47) The reduced value for n (number of electrons in the reduction process) is not due to changes in the diffusion coefficient (D) but rather reflects the fact that there is now 1 electron per $[(MoS_4)Fe_2Cl_3]^{2-}$ dimer. The possibility exists that there is a reduction in D; however, such a reduction is not expected to be significant.

(48) Nicholson, R. S.; Shain, I. *Anal. Chem.* **1964**, *36*, 706.

(49) The absence of concentration dependence evident in Figure 4 for the reduction of I does not argue against the formation of a dimer but rather indicates that the *rate-determining step* is first order in I in a process that could well be second order overall.

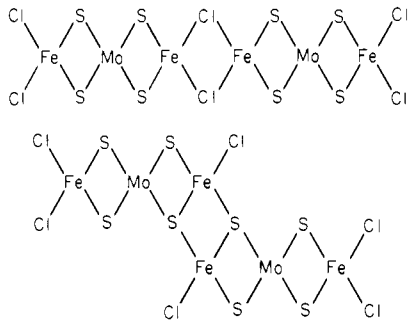

Figure 5. Possible structures for the $[MS_4Fe_2Cl_3^{2-}]_2$ anions.

VII). The first wave was diffusion controlled with a current function of 17 $\mu A/(V/s)^{1/2}$ mM, which at the HMDE corresponds to one electron. No reverse peak was seen for this wave. The heights of the second and third waves together corresponded to about one electron. An anodic wave was observed at +0.17 V vs. SCE. The additional cathodic waves that are observed in the voltammetry of $[Cl_2FeS_2WS_2FeCl_2]^{2-}$ appear to correspond to the waves observed in the reduction of $[MoS_4Fe_2Cl_3]^{2-}$. A likely interpretation of these results would be that the initial trianionic reduction product $[Cl_2FeS_2WS_2FeCl_2]^{3-}$ undergoes a much faster decomposition to $[WS_4Fe_2Cl_3]^{2-}$ than the molybdenum analogue. The difference of the peak potentials (240 mV) for the cathodic waves of the $[Cl_2FeS_2MS_2FeCl_2]^{2-}$ complexes (for M = Mo vs. W) supports the contention that the reduction is centered primarily on the molybdenum or tungsten atoms and is consistent with the Mössbauer data.

A possible structure for the $[MS_4Fe_2Cl_3]^{2-}$ complex anions must account for (a) the apparent dimeric nature of this compound suggested by the electrochemical results, (b) the bridging nature of the MS_4 group suggested by the infrared spectrum, and (c) the facile conversion to $[Fe(MoS_4)_2]^{3-}$ in coordinating solvents such as NMF. Two possible structures that are in compliance with the above restrictions are shown in Figure 5. Both of these structures contain two diffrent iron sites. The presence of single quadrupole doublets in the Mössbauer spectra of salts of the $[MS_4Fe_2Cl_3]^{2-}$ anions suggests either that the structures of I^- and II^- are different from any of those shown in Figure 5 or that the electronic differences between the two iron sites are too small to be resolved into two quadrupole doublets in the Mössbauer spectrum. The latter situation prevails in the Mössbauer spectra of structurally characterized mixed-ligand cubanes such as $[Fe_4S_4(SPh)_2Cl_2]^{2-}$ and $[Fe_4S_4(OPh)_2Cl_2]^{2-}$ that display only one quadrupole doublet in the Mössbauer spectra.[50]

Acknowledgment. This work has been supported generously by grants from the National Science Foundation (CHE-79-0389) and the National Institutes of Health (GM-26671-02).

Registry No. I, Ph_4P salt, 73621-80-4; I, Bu_4N salt, 88548-85-0; I, Et_4N salt, 88562-92-9; I^-, Et_4N salt, 88548-81-6; II, Ph_4P salt, 73621-82-6; II, Et_4N salt, 88562-93-0; II^-, Et_4N salt, 88548-83-8; $(Ph_4P)_2(Cl_2FeS_2MoS_2)$, 88548-73-6; $(Ph_4P)_2(Cl_2FeS_2WS_2)$, 88548-75-8; $(Ph_4P)_2[(PhS)_2FeS_2MoS_2]$, 88548-77-0; $(Ph_4P)_2[(PhS)_2FeS_2WS_2]$, 73493-04-6; $(Ph_4P)_2(Br_2FeS_2MoS_2FeBr_2)$, 88548-79-2.

Supplementary Material Available: Listings of positional and thermal parameters for all atoms and observed and calculated structure factors and a stereo drawing of the unit cell contents (76 pages). Ordering information is given on any current masthead page.

(50) Kanatzidis, M.; Coucouvanis, D.; Simopoulos, A.; Kostikas, A., manuscript in preparation.
(51) Johnson, C. K. "ORTEP", Report ORNL-3794; Oak Ridge National Laboratory: Oak Ridge, TN, 1965.

Contribution from the Department of Chemistry, Indiana University, Bloomington, Indiana 47405, and Department of Chemistry and Laboratory for Molecular Structure & Bonding, Texas A&M University, College Station, Texas 77843

Theoretical and Experimental Studies of the Electronic Structure of the $Mo_3(\mu_3\text{-}O)(\mu_3\text{-}OR)(\mu\text{-}OR)_3(OR)_6$ Type of Triangular Metal Atom Cluster Compound

MALCOLM H. CHISHOLM,*[1a] F. ALBERT COTTON,*[1b] ANNE FANG,[1b] and EDWARD M. KOBER[1a]

Received June 16, 1983

The electronic structure of a $Mo_3(\mu_3\text{-}O)(\mu_3\text{-}OR)(\mu\text{-}OR)_3(OR)_6$ molecule with R = H and C_{3v} symmetry, which serves as a model for real molecules in which R = $CH_2C(CH_3)_3$ or $CH(CH_3)_2$, has been calculated by the molecular orbital method of Hall and Fenske. The calculations have been performed not only on the entire molecule but on the Mo_3^{12+}, $Mo_3O(OH)^{9+}$, and $Mo_3O(OH)_4^{6+}$ fragments, and the metal–metal bonding has been tracked through these successive stages by the "clusters in molecules" formalism. In the full molecule the HOMO is an e orbital that carries most of the e-type M–M bonding while the a_1 type is carried by two MO's, one of which is quite stable. The LUMO is also an e-type orbital and the HOMO–LUMO gap is small (ca. 1.5 eV). It is predicted that the $MO_3O(OR)_{10}$ molecules of this type will have readily accessible redox chemistry in which both oxidation and reduction steps might be slow or irreversible, judging by the character of the HOMO and LUMO of the $Mo_3O(OR)_{10}$ molecule. Experimental observations on $Mo_3O(ONe)_{10}$, Ne = $CH_2C(CH_3)_3$, are in harmony with this. In addition, the absorption spectrum of $Mo_3O(ONe)_{10}$ has been observed, and an assignment based on the calculations is proposed.

Introduction

The group 6 elements molybdenum and tungsten show a remarkable predilection to form equilateral triangular metal atom cluster compounds,[2] and such clusters are also formed by other early transition elements[3] such as niobium.[4] Previous studies by Cotton and co-workers, in collaboration with colleagues in Haifa and Jerusalem, have provided experimental data as well as theoretical analyses[2,5] of compounds of the form $[M_3(\mu_3\text{-}X)_2(O_2CR)_6L_3]$, $[M_3(\mu_3\text{-}X)(\mu\text{-}Y)_3L_9]$, and $[M_3(\mu_3\text{-}X)(O_2CR)_6L_3]$. Theoretical work has also been done on related systems.[6,7]

(1) (a) Indiana University. (b) Texas A&M University
(2) For extensive references to earlier work both here and elsewhere, see ref 1–10 in: Ardon, M.; Cotton, F. A.; Dori, Z.; Fang, A.; Kapon, M.; Reisner, G. M.; Shaia, M. *J. Am. Chem. Soc.* **1982**, *104*, 5394.
(3) Müller, A.; Jostes, R.; Cotton, F. A. *Angew. Chem.* **1980**, *92*, 921; *Angew. Chem., Int. Ed. Engl.* **1980**, *19*, 875.
(4) Bino, A. *J. Am. Chem. Soc.* **1980**, *102*, 7990.
(5) Bursten, B. E.; Cotton, F. A.; Hall, M. B.; Najjar, R. C. *Inorg. Chem.* **1982**, *21*, 302.
(6) Cotton, F. A.; Fang, A. *J. Am. Chem. Soc.* **1982**, *104*, 113.
(7) Fang, A. Ph.D. Dissertation, Texas A&M University, 1982.

0020-1669/84/1323-0749$01.50/0